REPORT DOCUMENTATION PAGE

Form Approved
OMB No. 0704-0188

1. REPORT DATE *(DD-MM-YYYY)* 26-10-2011	**2. REPORT TYPE** Briefing Charts	**3. DATES COVERED** *(From - To)*

4. TITLE AND SUBTITLE

Proper Orthogonal Decomposition Analysis of Shear-Coaxial Injector Flows with or Without Transverse Acoustic Forcing

5a. CONTRACT NUMBER

5b. GRANT NUMBER

5c. PROGRAM ELEMENT NUMBER

6. AUTHOR(S)

Sophonias Teshome, Ivett A. Leyva and Douglas Talley

5d. PROJECT NUMBER

5f. WORK UNIT NUMBER

23080533

7. PERFORMING ORGANIZATION NAME(S) AND ADDRESS(ES)

Air Force Research Laboratory (AFMC)
AFRL/RZSA
10 E. Saturn Blvd.
Edwards AFB CA 93524-7680

8. PERFORMING ORGANIZATION REPORT NUMBER

AFRL-RZ-ED-VG-2011-435

9. SPONSORING / MONITORING AGENCY NAME(S) AND ADDRESS(ES)

Air Force Research Laboratory (AFMC)
AFRL/RZS
5 Pollux Drive
Edwards AFB CA 93524-7048

10. SPONSOR/MONITOR'S ACRONYM(S)

11. SPONSOR/MONITOR'S NUMBER(S)

AFRL-RZ-ED-VG-2011-435

12. DISTRIBUTION / AVAILABILITY STATEMENT

Approved for public release; distribution unlimited (PA #11929).

13. SUPPLEMENTARY NOTES

For presentation at the JANNAF 2011 Joint Subcommittee Meeting, Huntsville, AL, 5-9 Dec 2011.

14. ABSTRACT

This experimental study investigated the response of dynamic flow structures of cryogenic coaxial nitrogen jets to pressure perturbations due to transverse acoustic forcing at a pressure antinode (PAN). The role of injector exit geometry on the flow response was examined using two shear coaxial injectors with different outer-to-inner jet area ratios. Flow conditions spanning subcritical (reduced pressure of 0.44) to supercritical (reduced pressure of 1.05) chamber pressures, varying outer-to-inner jet momentum flux ratios (0.5 – 20), and acoustic pressure antinode at the jet axis location were considered. A basic application of proper orthogonal decomposition on the intensity fluctuation of high-speed images enabled the extraction of the spatial and temporal characteristics of the dominant flow structures that existed in the flow field during exposure to acoustic forcing. Regardless of injector geometry or pressure regime, low outer-to-inner momentum flux ratio flows were found to be responsive to acoustic pressure antinode forcing. With increasing momentum flux ratio, however, the flow response to forcing depended on the injector geometry.

15. SUBJECT TERMS

16. SECURITY CLASSIFICATION OF:			**17. LIMITATION OF ABSTRACT**	**18. NUMBER OF PAGES**	**19a. NAME OF RESPONSIBLE PERSON** Dr. Douglas Talley
a. REPORT **Unclassified**	**b. ABSTRACT** **Unclassified**	**c. THIS PAGE** **Unclassified**	SAR	29	**19b. TELEPHONE NUMBER** *(include area code)* N/A

Standard Form 298 (Rev. 8-98)
Prescribed by ANSI Std. 239.18

Proper Orthogonal Decomposition Analysis of Shear-Coaxial Injector Flows with and without Transverse Acoustic Forcing

Sophonias Teshome[†], Ivett A. Leyva[‡], Douglas Talley[‡]

[†]UCLA/Edwards AFRL, [‡]Edwards AFRL

JANNAF 8th Modeling and Simulation/6th Liquid Propulsion/5th Spacecraft Propulsion Subcommittees Meeting

December 5, 2011

Motivation

- Feedback cycle between liquid rocket engine (LRE) combustion chamber pressure perturbations and unsteady combustion[1,2]
- Large amplitude fluctuations in pressure and combustion heat release rates ⇒ combustion instability

[1]Harrje, D.T., and Reardon, F.H.. *Scientific and Technical Information Office*, National Aeronautics and Space Administration, NASA SP-194, 1972.

[2]Schadow, K.C., Gutmark, E., Parr, T.P., Parr, D.M., Wilson, K.J., and Crump, J.H.. *19th AIAA Fluid Dynamics, Plasma Dynamics and Lasers Conference*, AIAA 1987-1326

Objective

- Impose external acoustic perturbations, and examine the response and stability characteristic of shear-coaxial injector flow to pressure perturbation

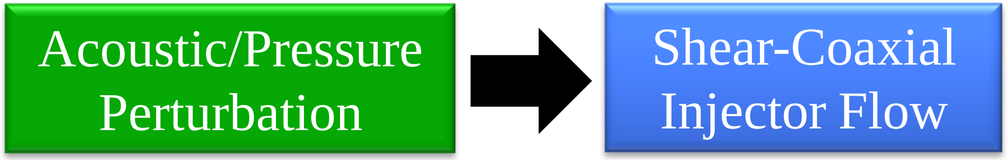

- Investigate influence of injector geometry on flow response to external pressure perturbation
- Vary the outer-to-inner jet momentum flux ratio, *J*, under subcritical and nearcritical chamber pressure conditions, i.e., reduced pressures *Pr* = 0.44, 1.05

$$J = \frac{\rho_o u_o^2}{\rho_i u_i^2} \qquad Pr = \frac{P_{chamber}}{P_{critical,\mathrm{N}_2}} \qquad P_{critical,\mathrm{N}_2} = 493\,\mathrm{psi}\,(3.4\,\mathrm{MPa})$$

- Apply proper orthogonal decomposition of high-speed image pixel intensity fluctuations to extract spatial and temporal characteristics of prevalent coherent flow structures

Previous Works on Jet Instability

- Michalke and Hermann (1982) did linear, inviscid instability analysis of a circular jet with coflow
- Showed that with increasing coflow velocity, U_∞
  - Helical disturbances more unstable than axisymmetric ones farther downstream of exit
  - Jet flow becomes less unstable, but spectrum of spatial growth rate becomes broader and the peak shifts to higher frequencies

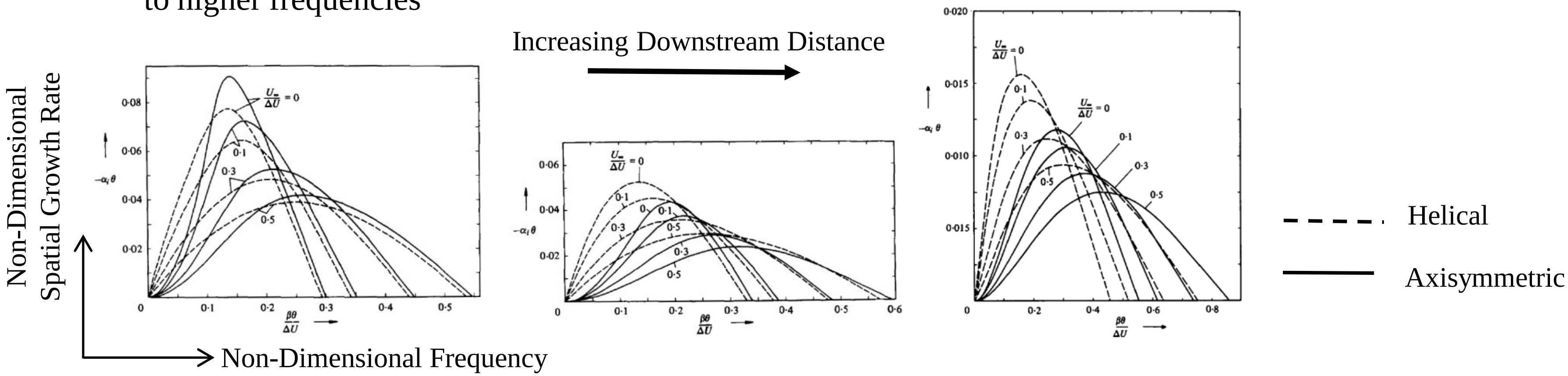

- Dahm *et al.* (1992), Wicker and Eaton (1994) conducted experimental investigation of large-scale vortex structures in the near field of coaxial jets
  - For outer-to-inner jet velocity ratios greater than one, found that coherent structures in the outer shear layer dominate those in the inner shear layer
  - At large axial distances, shear-layer vortices exhibit helical structures

Dahm *et al.*, *JFM* 1992

Schematic of Experimental Facility

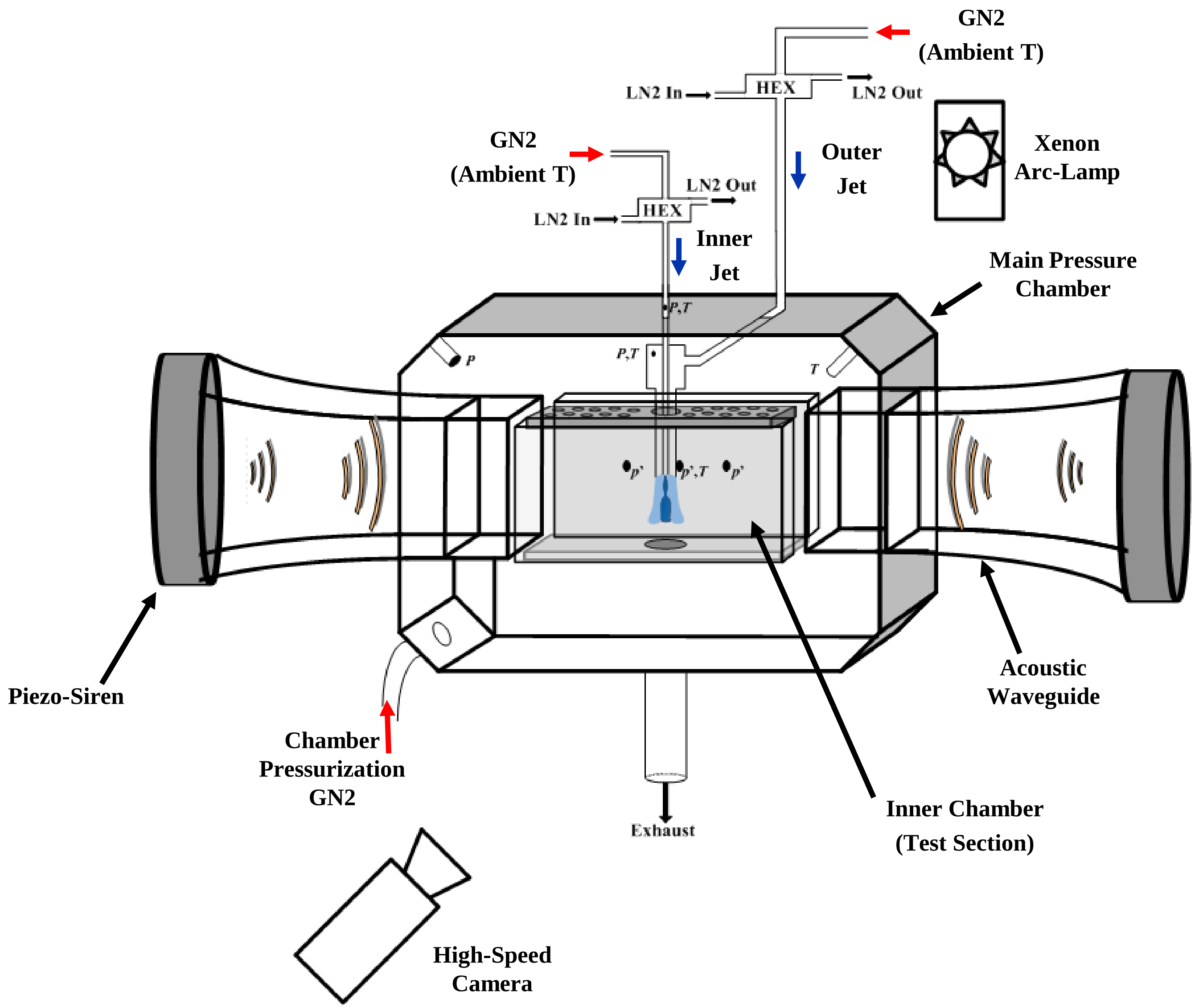

Image of Experimental Facility

Piezo-Siren

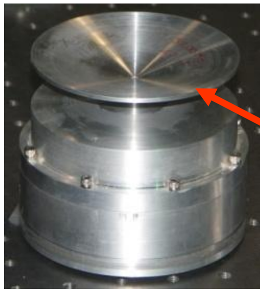

Waveguide

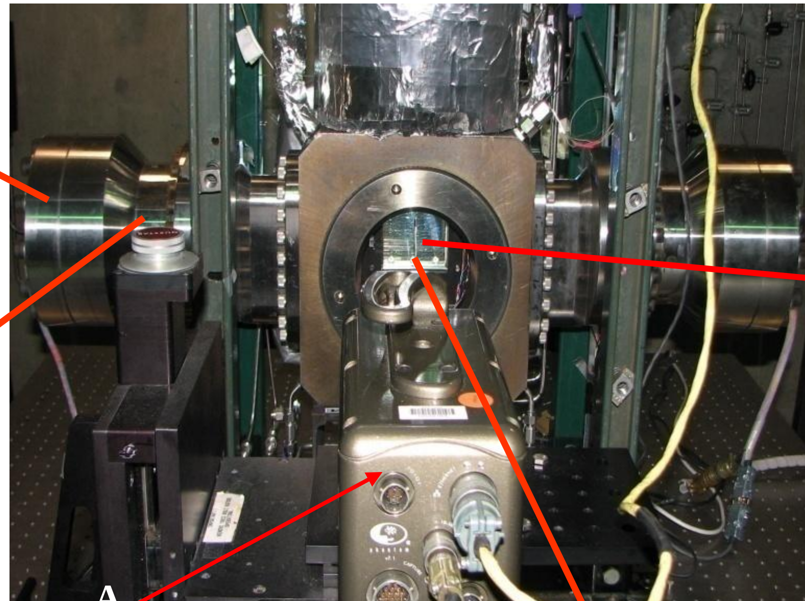

Thermocouple Probe

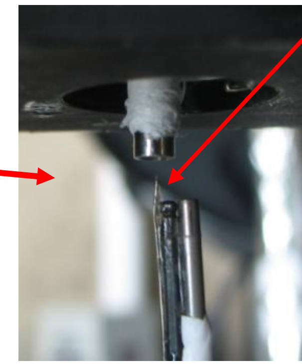

High-Speed Camera

Coaxial Injector

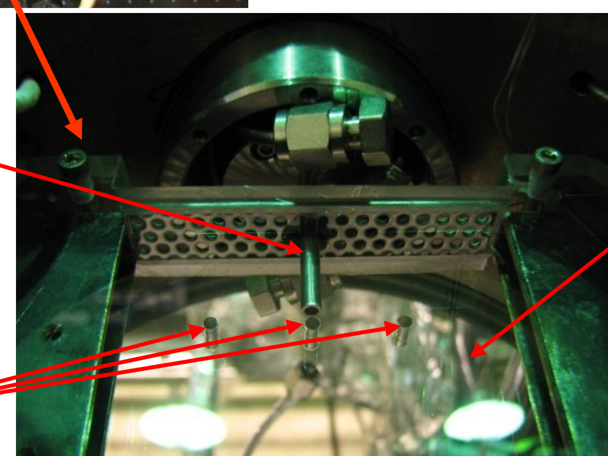

Inner Chamber

Differential Pressure Transducers

Injector Configuration

- Two types of outer-to-inner jet cross-sectional area ratios
  - Large Area Ratio (LAR)
  - Small Area Ratio (SAR)

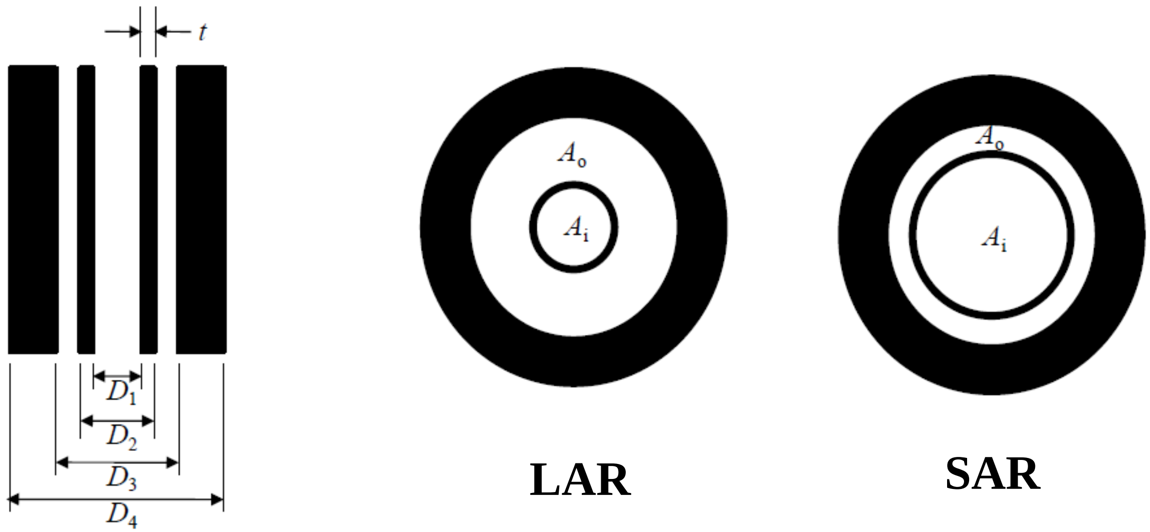

Injector	t	D_1	t/D_1	D_2	D_3	D_4	A_o/A_i
LAR	0.09	0.70	0.13	0.89	2.44	3.94	10.6
SAR	0.13	1.40	0.09	1.65	2.44	3.94	1.65

Acoustic Field Set-Up: Pressure Antinode

- Pressure antinode (PAN) – condition of maximum pressure perturbation in the acoustic field
- Piezo-sirens forced in-phase
- Superposition of quasi-1D acoustic waves traveling in opposite directions ⇒ PAN at the jet location (geometric center of test section)

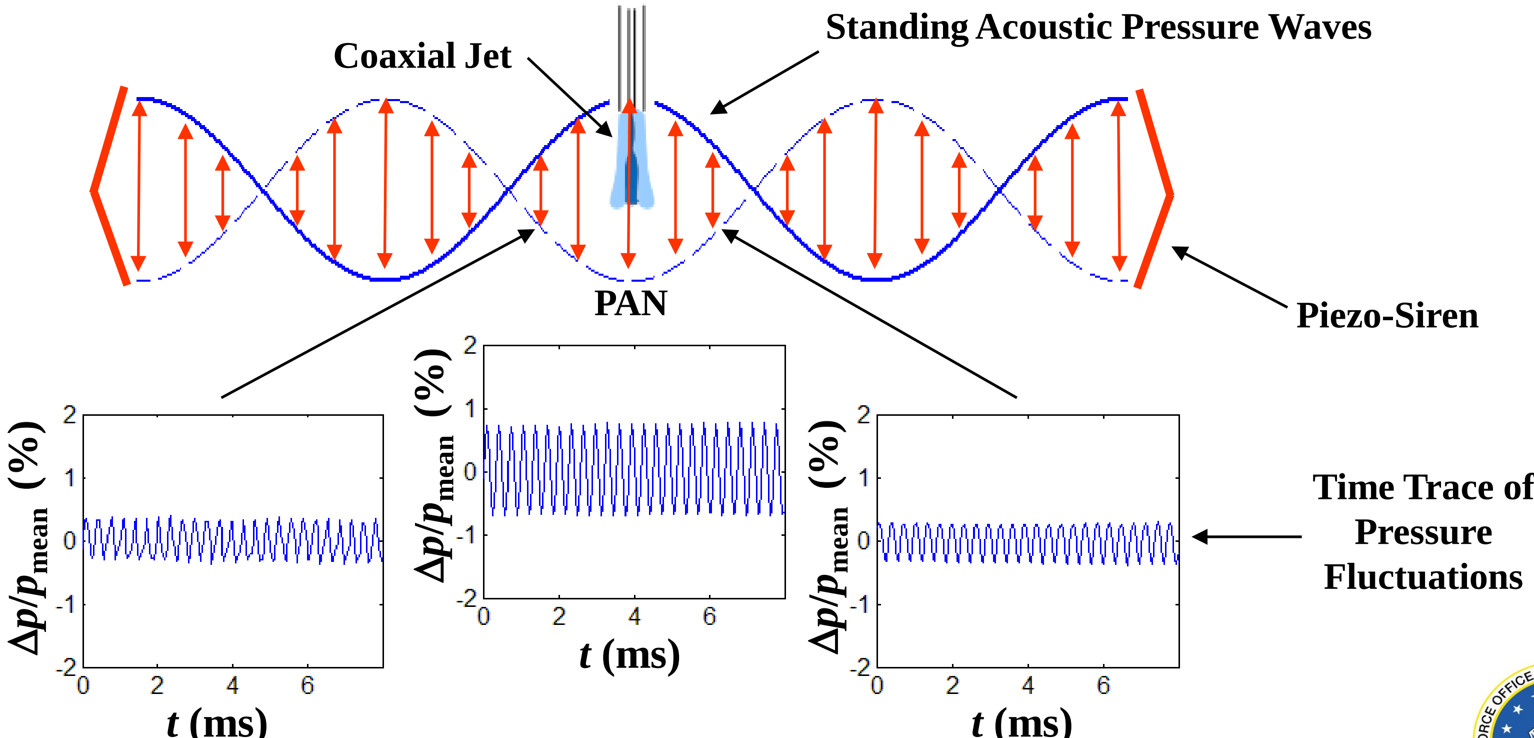

Proper Orthogonal Decomposition

• Proper Orthogonal Decomposition (POD) or Principal Component Analysis (PCA) was used for extracting dominant dynamical processes embedded in high-speed images.

• A time-resolved set of images $A(x,t)$ can be represented as a linear combination of orthonormal basis functions ϕ_k (aka proper orthogonal modes)[1,2] :

$$A(x,t) = \sum_{k=1}^{M} a_k(t)\phi_k(x)$$

where $a_k(t)$ are time dependent orthonormal amplitude coefficients and M is the number of modes

• Main idea: POD modal amplitudes capture the maximum possible "energy" in an average sense[3], i.e.,

$$\sum_k \langle a_k(t)a_k(t)\rangle \geq \sum_k \langle b_k(t)b_k(t)\rangle$$

where $b_k(t)$ are the temporal coefficients of a decomposition with respect to an arbitrary orthonormal basis ψ_k.

[1] **Chatterjee, A**. *Current Science*, Vol. 78, No. 7 (2000)
[2] **Arienti, M, and Soteriou, M.C.**. Phys. Fluids 21, 112104 (2009)
[3] **Narayanan,V., Lightfoot, M.D.A, Schumaker, S.A., Danczyk, S.A.,** and **Eilers, B.**. *ILASS Americas*, 2011
[4] **Berkooz, G., Holmes, P., and Lumley, J.L.**. *Annu. Rev. Fluid Mech.* 25. 539 (1993)

Construction of Data Set

• First, form a row vector consisting of all pixel intensity values of each snapshot image (with resolution of *n* rows by *m* columns) in order of increasing columns, then increasing rows

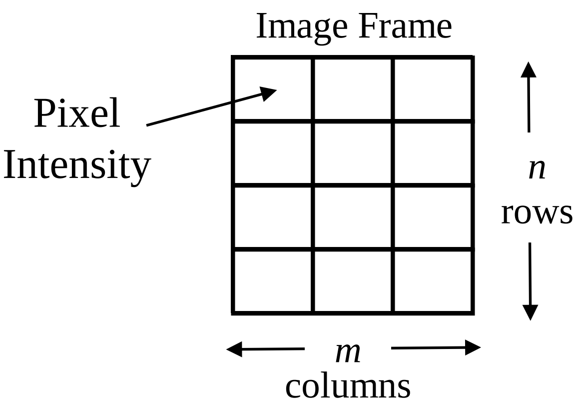

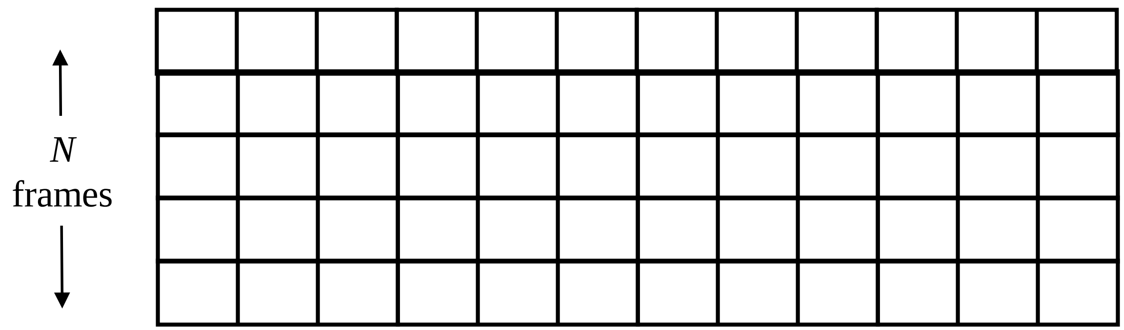

• Then, combine all such row vectors for *N* sequences of image frames resulting in a matrix **A** consisting of *N* rows by $P = n \times m$ columns of intensity values.

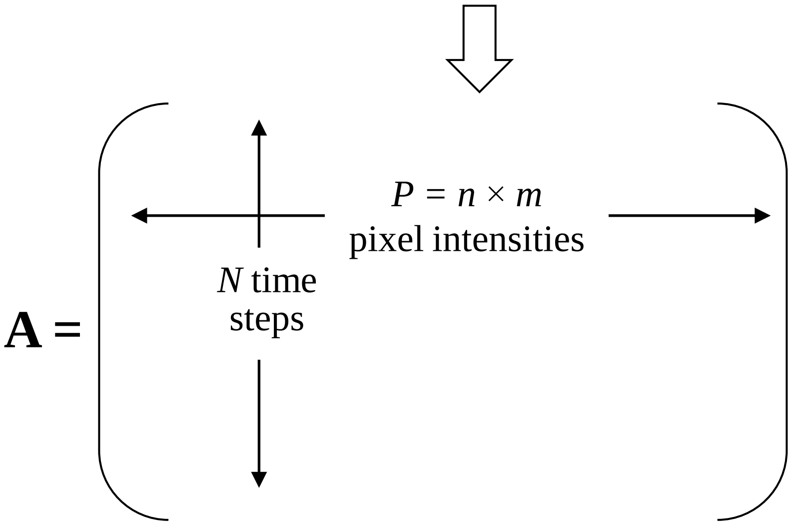

Orthogonal Decomposition Technique

- Eigenvalue decomposition or singular value decomposition (SVD) can be used
- SVD preferred since
    1. Applicable to non-square matrices (most likely the case)
    2. Decomposition matrices are orthogonal
    3. Subroutine readily available in MATLAB®
- Subtracted temporal mean of $\mathbf{A} \Rightarrow$ matrix of intensity fluctuations $\tilde{\mathbf{A}}$
- Applied SVD

$$\Rightarrow \tilde{\mathbf{A}} = \mathbf{U}\mathbf{S}\mathbf{V}^{\mathrm{T}} = \mathbf{Q}\mathbf{V}^{\mathrm{T}}$$

Columns of $\mathbf{Q} \sim a_k(t)$ contain temporal information

Columns of $\mathbf{V} \sim \phi_k(x)$ contain spatial information

$\mathbf{U}$: $N \times N$

Orthogonal Matrix of Left Singular Column Vectors of $\tilde{\mathbf{A}}$

$\mathbf{S}$: $N \times N$

Diagonal Matrix of Singular Values

$\mathbf{V}$: $N \times P$

Orthogonal Matrix of Right Singular Column Vectors of $\tilde{\mathbf{A}} \Leftrightarrow$ proper orthogonal modes (POM)

Results – Subcritical Baseline at Low *J*

- LAR, $Pr = 0.44$, $J = 0.5$

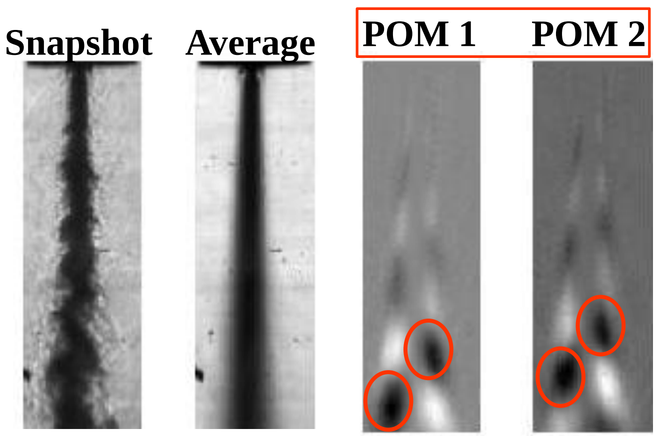

Amplitude information contained in singular values

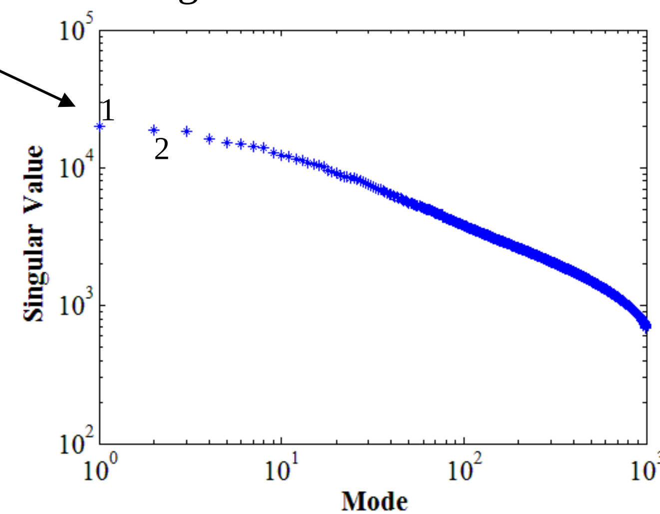

Antisymmetric Structures Identified with Characteristic Frequencies

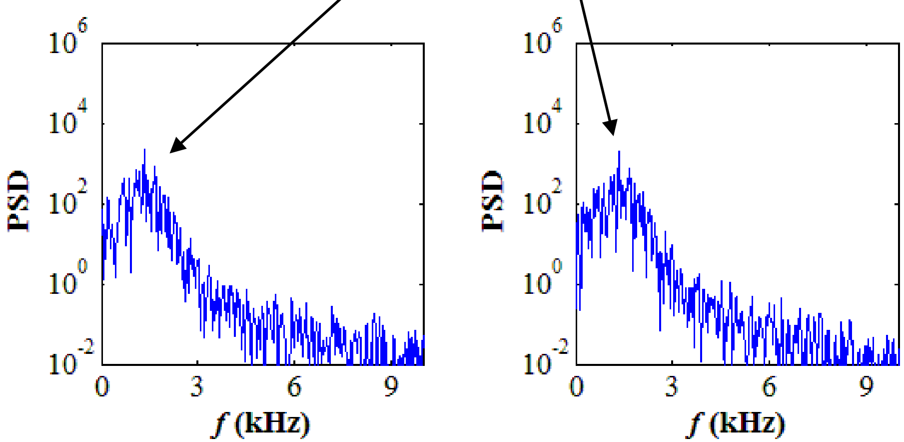

Power Spectral Densities (PSD) of Temporal Coefficients of POMs 1 and 2

Results – Subcritical PAN at Low J

- LAR, $Pr = 0.44$, $J = 0.5$, forcing Frequency, $f_F = 3.14$ kHz

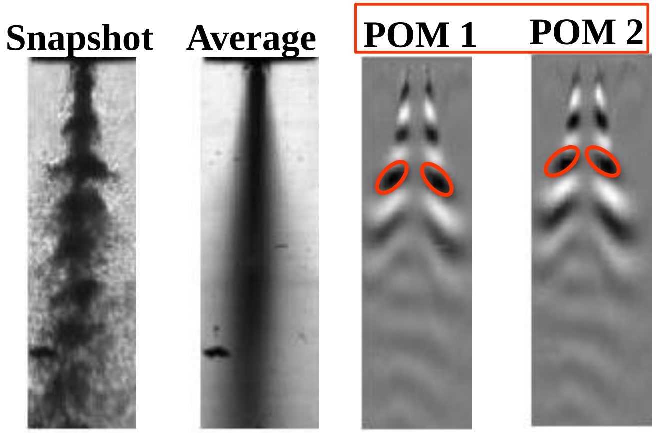

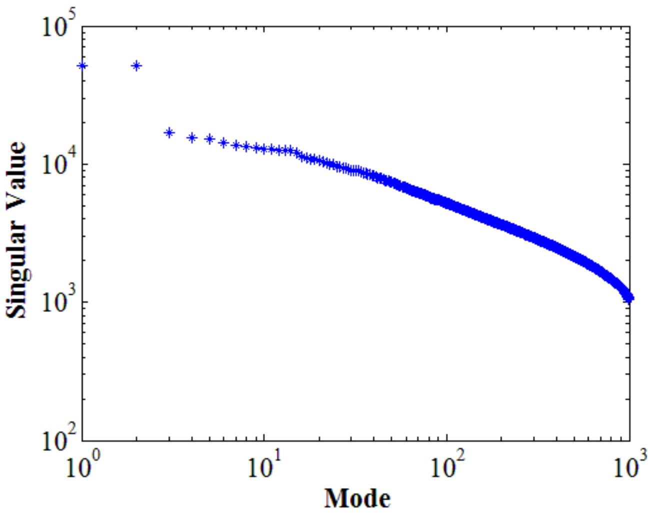

Symmetric Structures
Identified with Characteristic
Frequency at $\boldsymbol{f_F}$

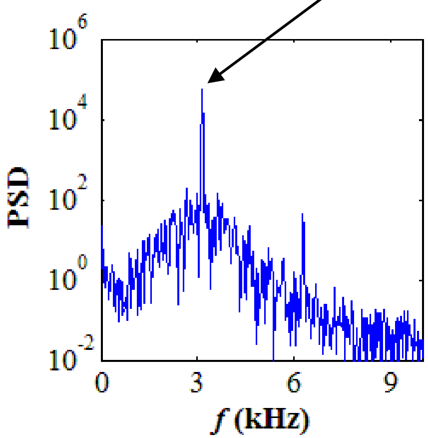

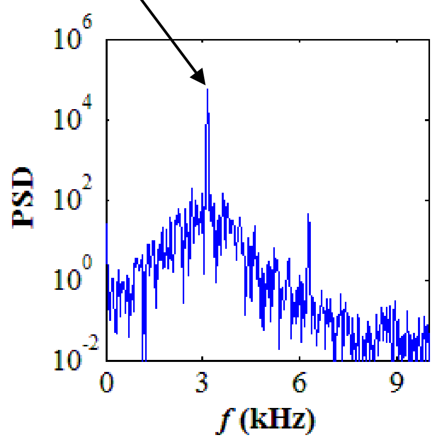

Cross-Power Spectral Density (CPSD)

- CPSD yields the FFT of the cross-correlation of the temporal coefficients
- Magnitude and phase plots used to determine existence of propagating structures

<u>LAR, $Pr = 0.44$, $J = 0.5$</u>

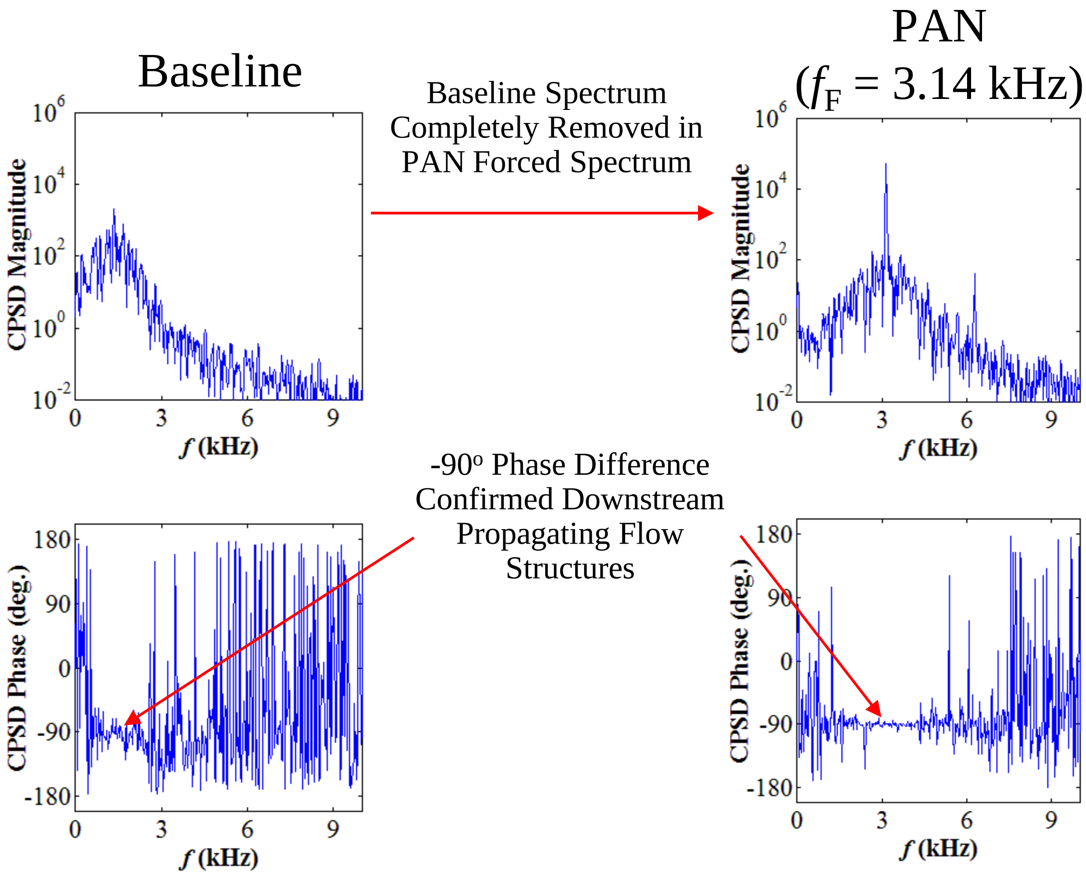

Sample Animation – PAN (f_F = 3.14 kHz)

- LAR Pr = 0.44, J = 0.5

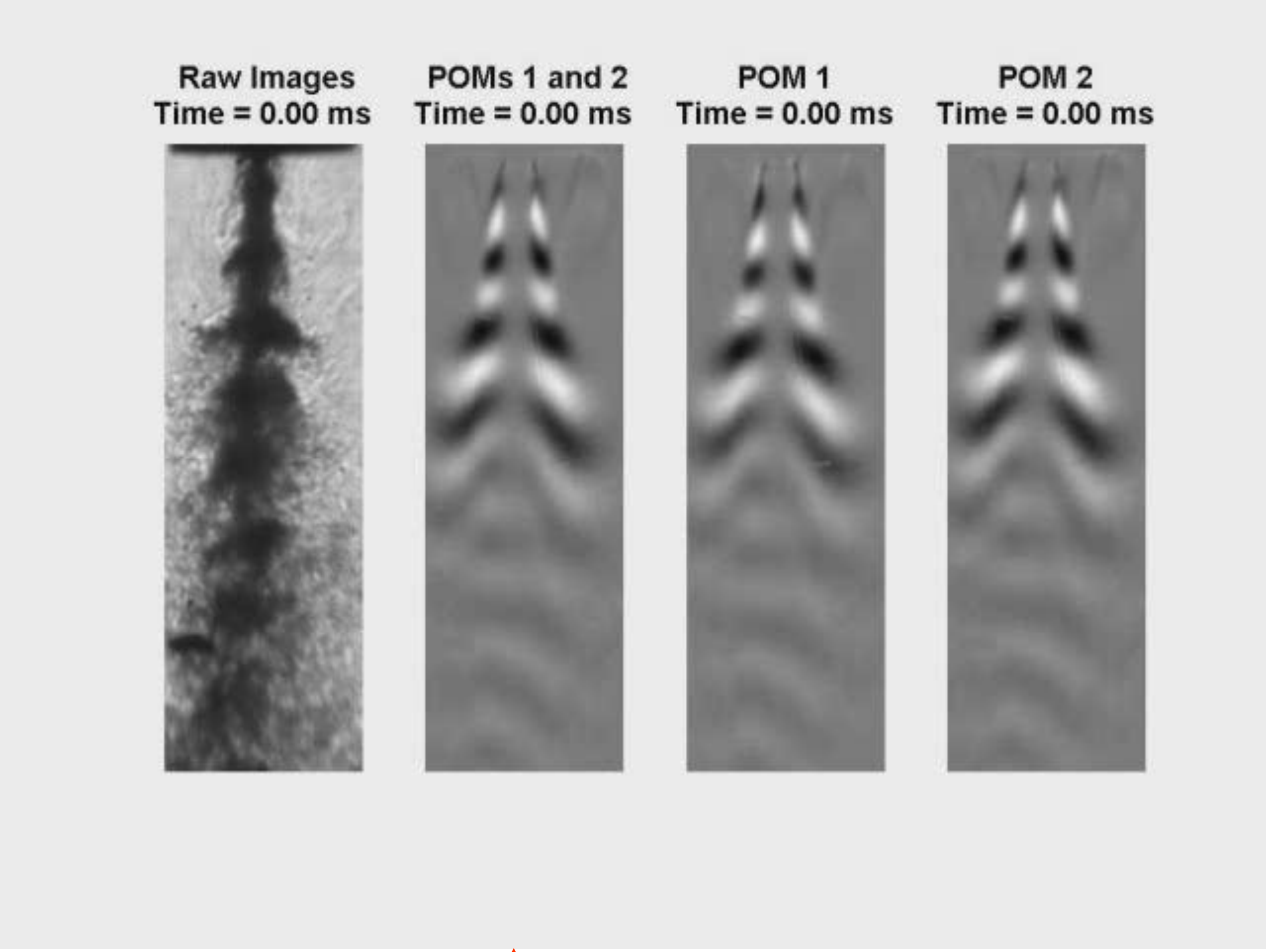

Superposition of POMs 1 and 2 Resulted in Downstream Propagating Structures

Results – LAR, *Pr* = 0.44, Baseline

- Antisymmetric flow structures indicated helical type flow instabilities for all *J*

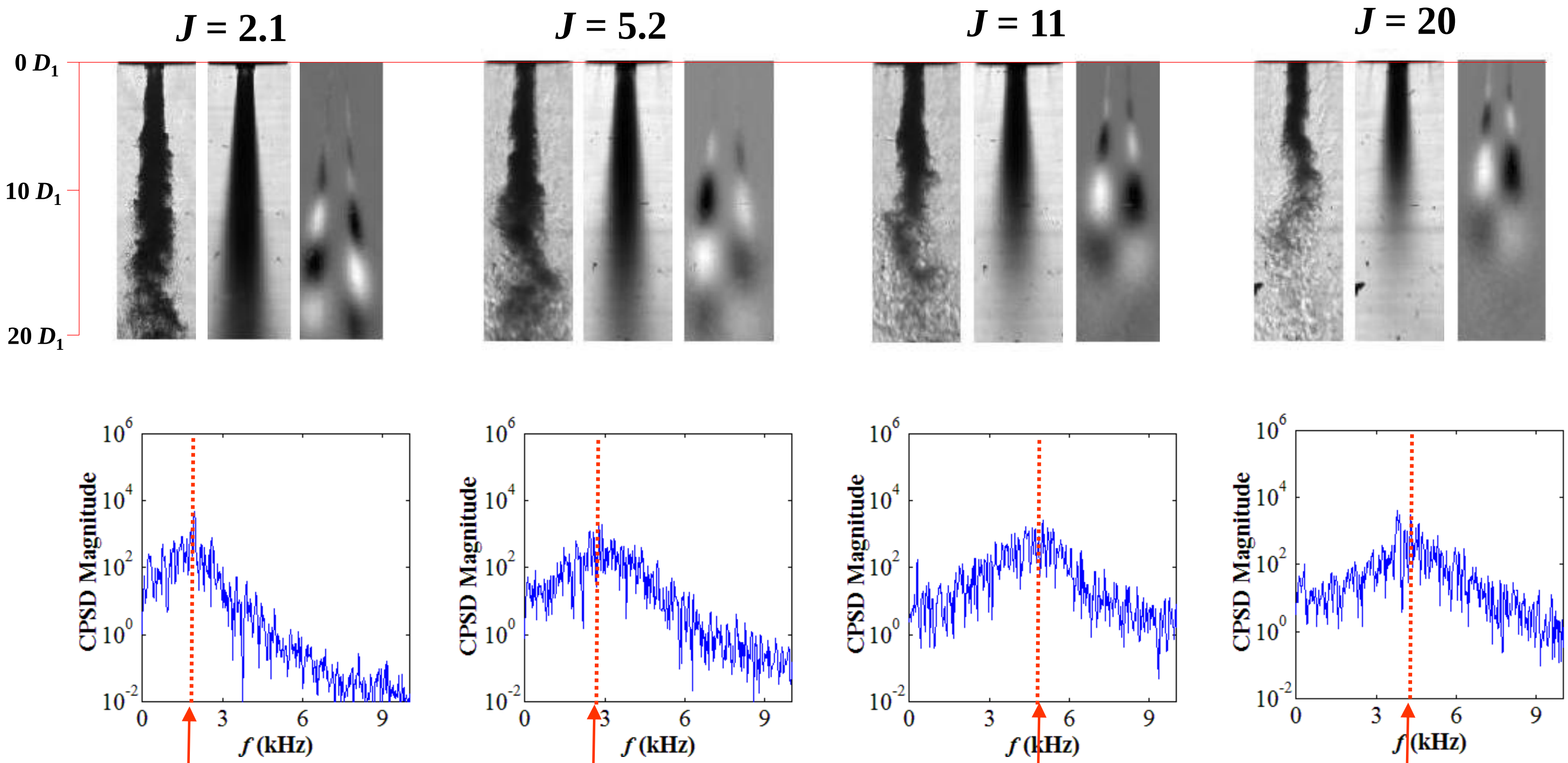

Characteristic peaks broadened and shifted to higher frequencies with increasing outer jet velocity

Results – LAR, *Pr* = 0.44, PAN

- Gradual shift from symmetric to antisymmetric flow structures with increasing J
- Response at forcing frequency, f_F, dominant at lower J

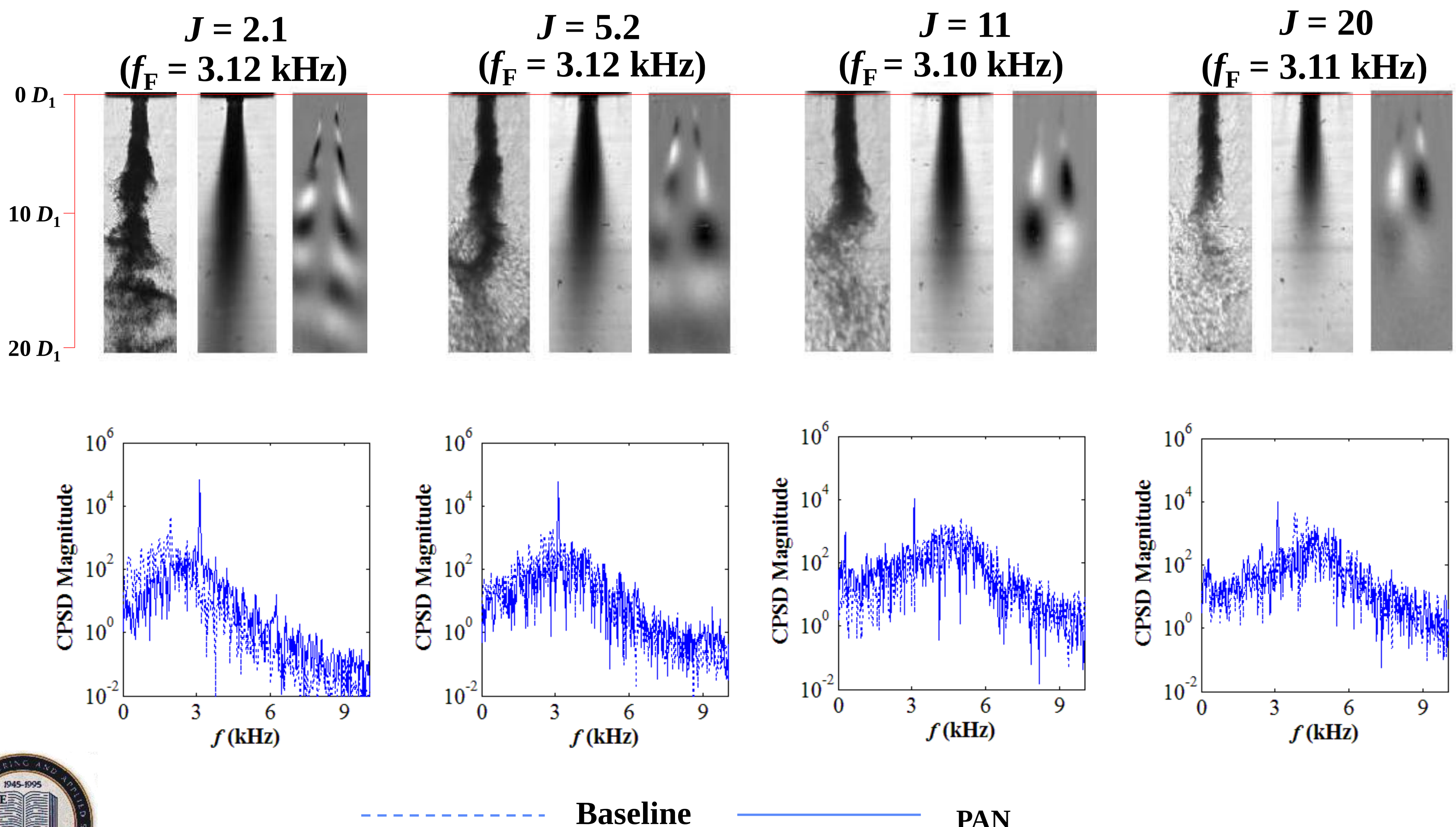

Results – LAR, *Pr* = 1.05, Baseline

- Antisymmetric flow structures indicated helical type flow instabilities for all *J*

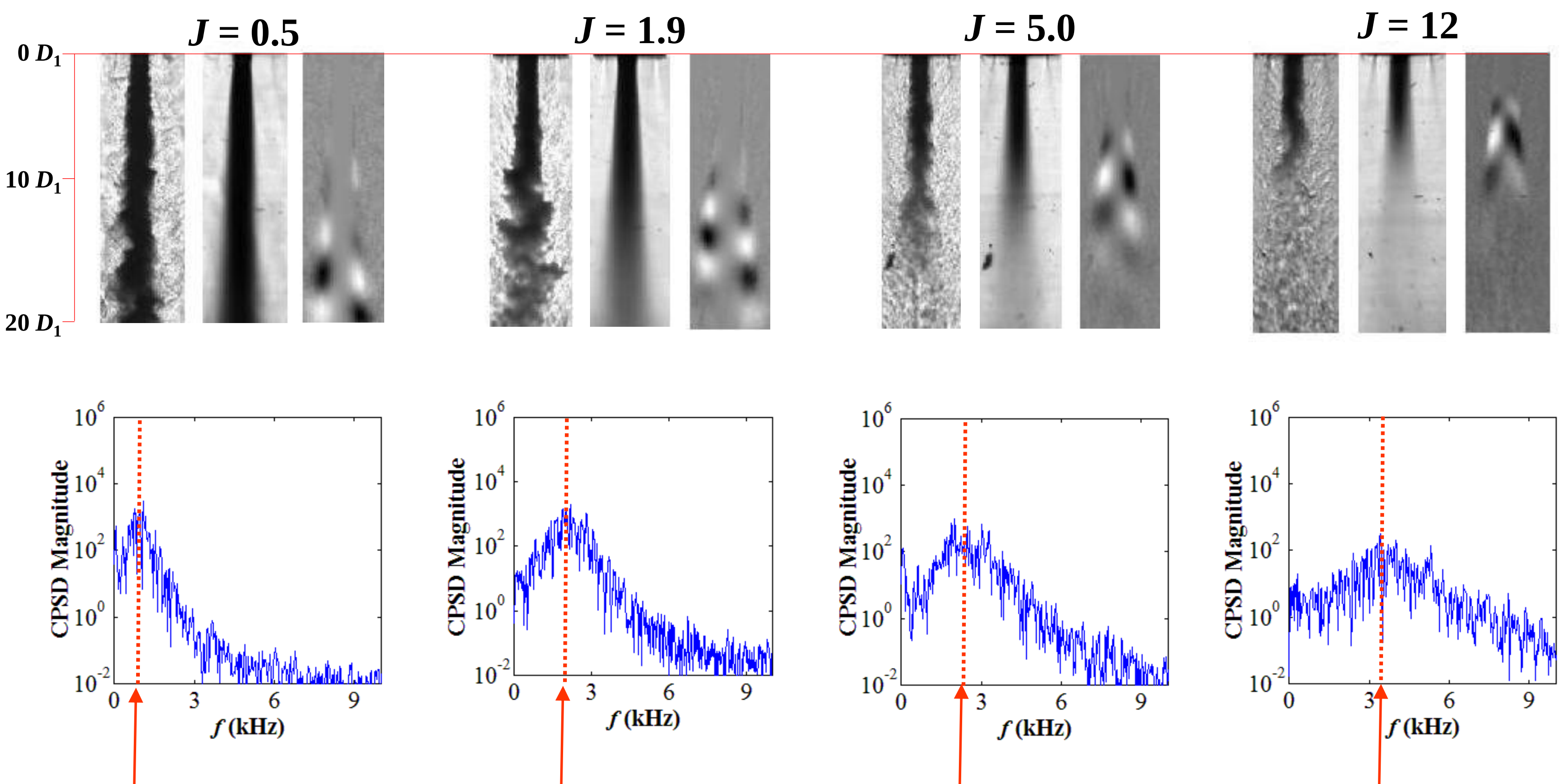

Similar to *Pr* = 1.05, peaks broadened and shifted to higher frequencies with increasing outer jet velocity

Results – LAR, *Pr* = 1.05, PAN

- Trend in response with varying *J* similar to *Pr* = 0.44
- Gradual shift from symmetric to antisymmetric flow structures with increasing *J*
- Response at f_F still took over natural (baseline) frequency at lower *J*

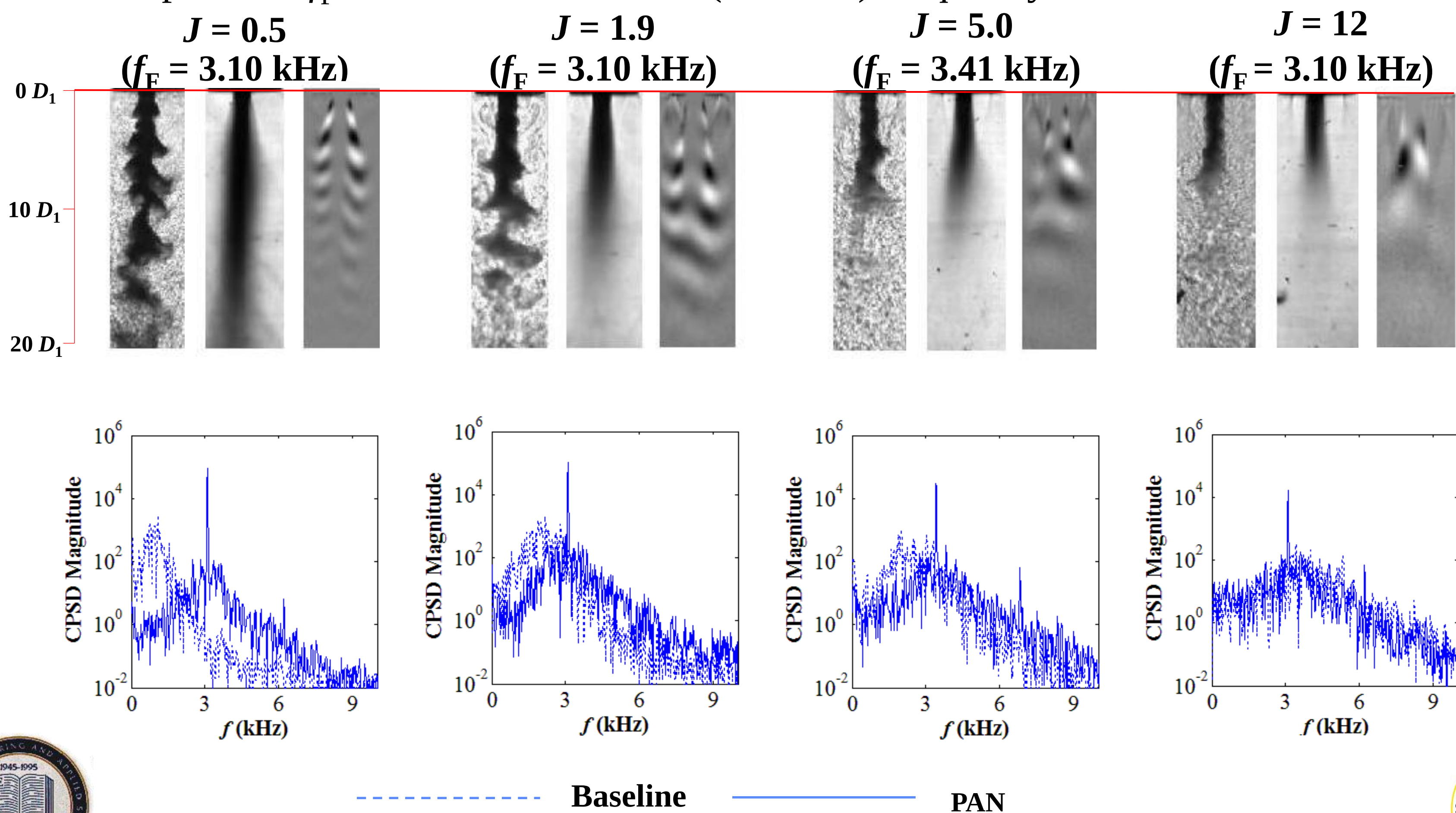

Results – SAR, *Pr* = 0.44, Baseline

- Helical type flow instabilities became more well-defined with increasing *J*

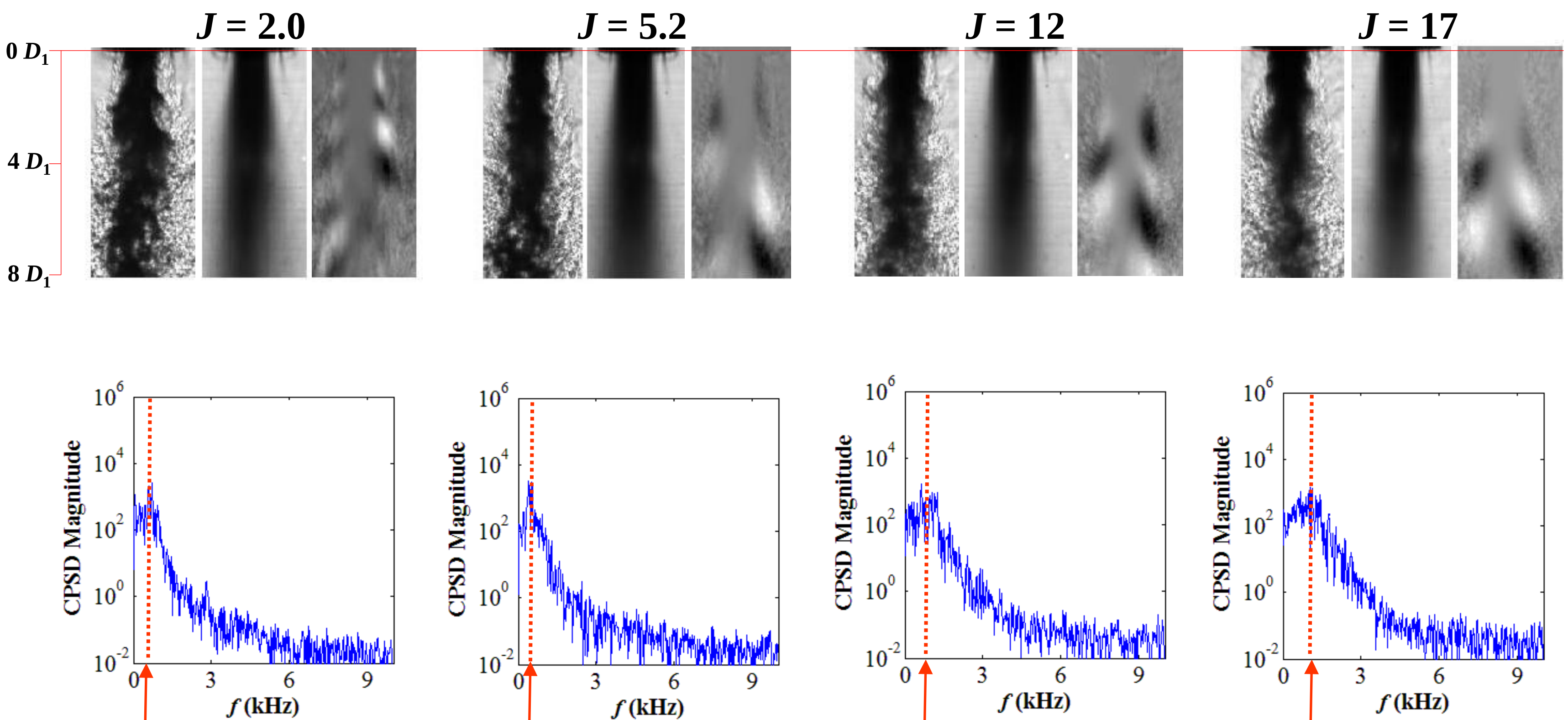

Unlike LAR flows, characteristic peaks showed minimal variation in frequency with outer jet velocity

Results – SAR, *Pr* = 0.44, PAN

- Symmetric structures persist despite increasing J
- Response at f_F strong at highest J

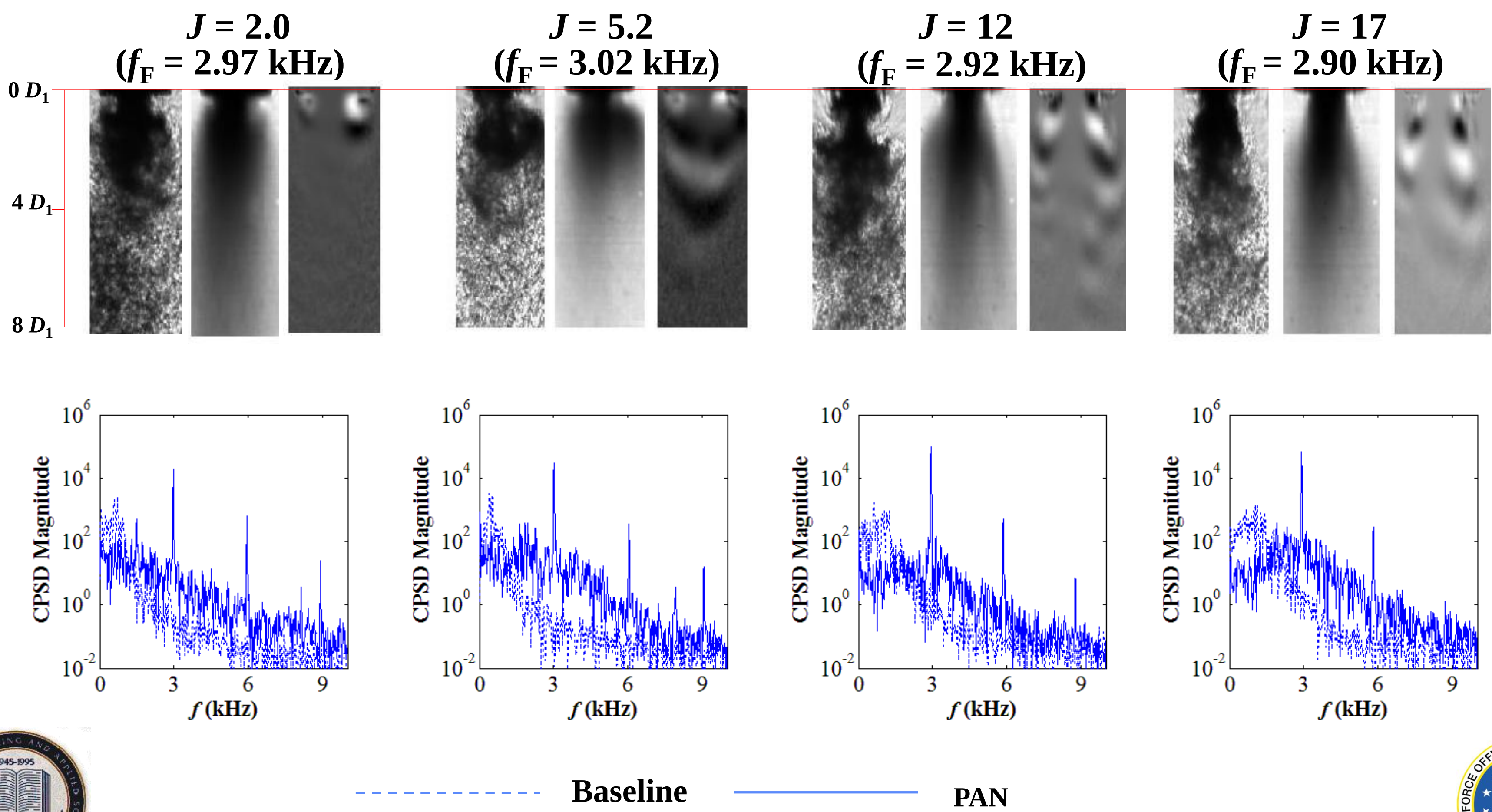

Results – SAR, *Pr* = 1.05, Baseline

- Antisymmetric flow structures indicated helical type flow instabilities

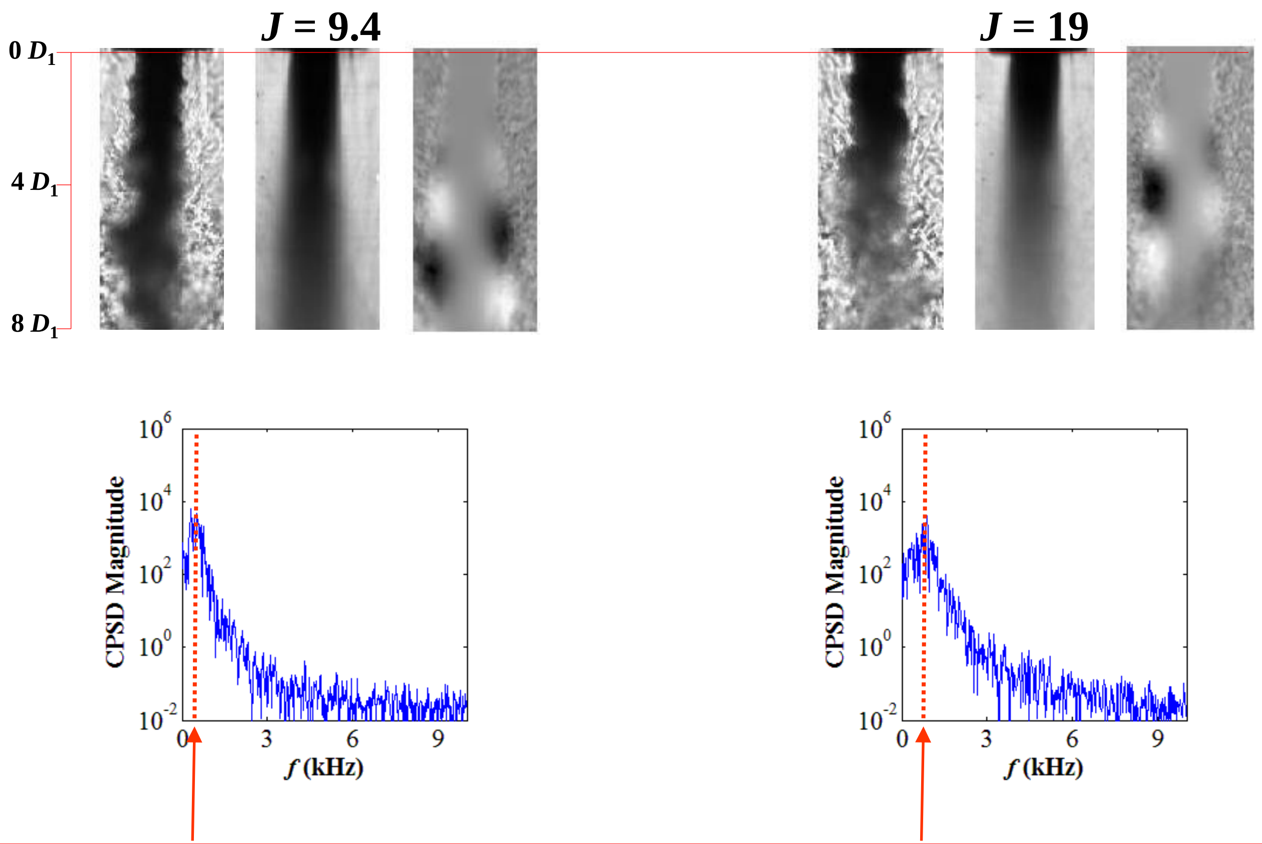

Similar to *Pr* = 0.44, characteristic peaks showed minimal variation in frequency with increasing outer jet velocity

Results – SAR, *Pr* = 1.05, PAN

- Similar to *Pr* = 0.44, symmetric structures persist even at high *J*
- Vortex-pairing interactions were most dominant response at $0.5f_F$
- Response at f_F strong at highest *J*

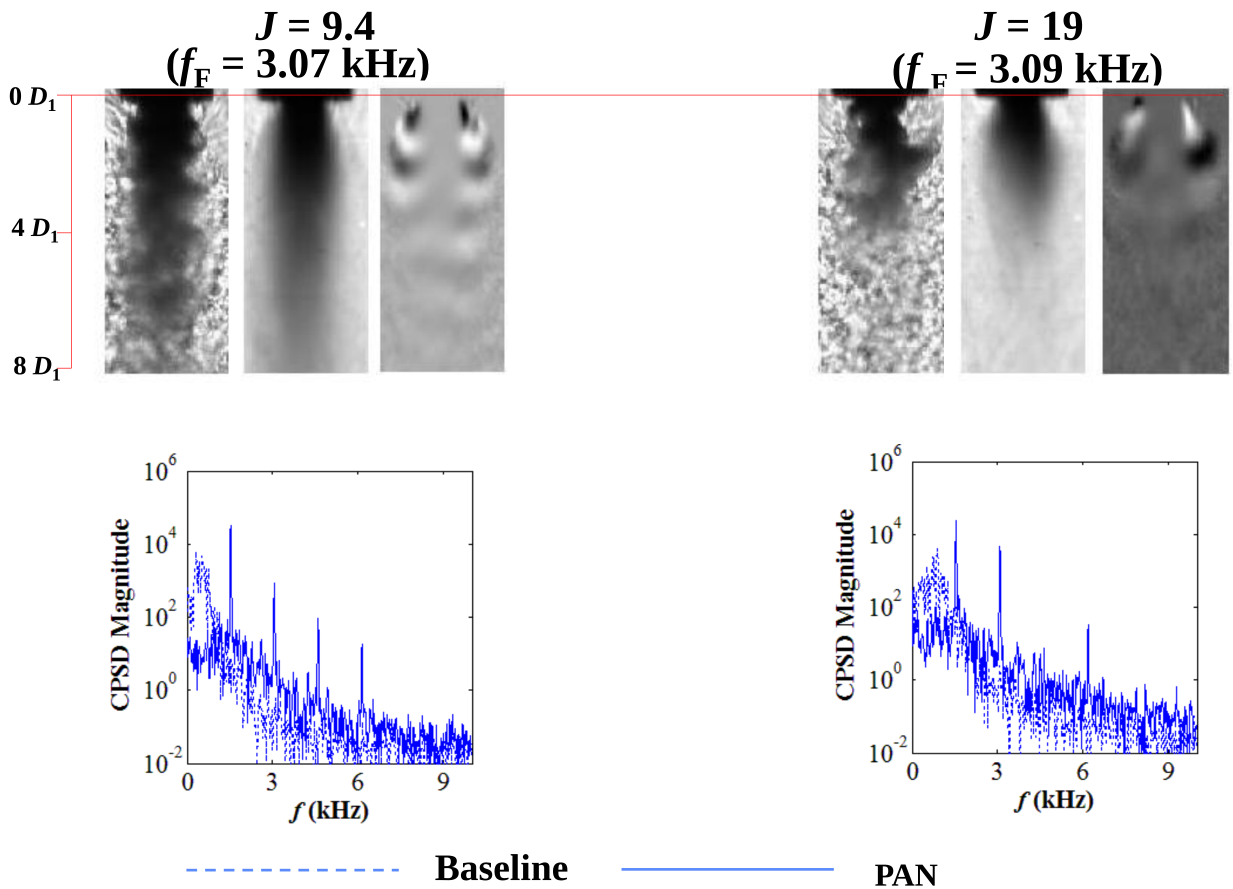

Conclusion

- **Proper orthogonal decomposition** of high-speed image **intensity fluctuation** data revealed key **spatial** and **temporal characteristics** of flow structures
- In both pressure regimes, **LAR** injector:
  - Peak frequencies of baseline flow instabilities became broader and shifted to higher frequencies with increasing *J*
  - PAN forcing at low *J* produced symmetric flow structures, while at higher *J*, influence of forcing subsided
  - Spectral magnitude plots showed **decreasing influence of PAN** forcing with **increasing *J***
- In both pressure regimes, SAR injector:
  - Increasing *J* had minimal influence on peak frequencies of baseline flow instabilities
  - PAN forcing produced symmetric flow structures regardless of *J*
  - Spectral plots showed **strong response** to **PAN** forcing at **low and high *J***
- Operated at **high** enough ***J***, **LAR** injector flows **less vulnerable to external pressure disturbances**

Acknowledgement

- Mechanical Crew
  - Randy Harvey, David Hill, Earl Thomas (ERC)
  - Todd Newkirk (Jacobs Engineering)
- Discussion and Advice
  - Prof. Ann Kargozian (UCLA Department of Mechanical and Aerospace Engineering)
- Discussion and SAR Data
  - Dr. Juan Rodriguez
- This work is sponsored by the Air Force Office of Scientific Research under Dr. Mitat Birkan, program manager.

Back-Up Slides

Data Summary Tables - LAR

$Pr = 0.44$, LAR

J	R	$T_{chamber}$ (K)	$\rho_{chamber}$ (kg/m^3)	$P_{chamber}$ (MPa)	T_{outer} (K)	$\dot{m}_{outer}$ (mg/s)	ρ_{outer} (kg/m^3)	u_{outer} (m/s)	Re_{outer} (10^4)	T_{inner} (K)	$\dot{m}_{inner}$ (mg/s)	ρ_{inner} (kg/m^3)	u_{inner} (m/s)	Re_{inner} (10^4)
0.5	3.5	217	24	1.50	204	1106	26	10.7	3.1	110	727	622	3.0	2.4
2.1	7.4	220	23	1.50	205	2212	25	21.5	6.3	107	725	646	2.9	2.1
5.2	11	221	23	1.50	203	3531	26	33.9	10	108	733	639	3.0	2.2
11	17	216	24	1.51	204	4991	26	47.9	14	107	722	646	2.9	2.1
20	22	220	23	1.50	204	4633	26	44.8	13	110	482	622	2.0	1.6

$Pr = 1.05$, LAR

J	R	$T_{chamber}$ (K)	$\rho_{chamber}$ (kg/m^3)	$P_{chamber}$ (MPa)	T_{outer} (K)	$\dot{m}_{outer}$ (mg/s)	ρ_{outer} (kg/m^3)	u_{outer} (m/s)	Re_{outer} (10^4)	T_{inner} (K)	$\dot{m}_{inner}$ (mg/s)	ρ_{inner} (kg/m^3)	u_{inner} (m/s)	Re_{inner} (10^4)
0.5	2.1	223	56	3.56	199	1742	65	6.6	4.8	115	724	605	3.1	2.5
1.9	4.1	221	57	3.56	200	3479	65	13.3	9.6	118	724	577	3.3	2.8
5.0	6.5	223	57	3.58	203	4189	64	16.2	11	122	511	531	2.5	2.4
12	9.9	223	56	3.57	208	6217	62	24.9	17	124	482	497	2.5	2.5

Data Summary Tables - SAR

$Pr = 0.44$, SAR

J	R	$T_{chamber}$ (K)	$\rho_{chamber}$ (kg/m^3)	$P_{chamber}$ (MPa)	T_{outer} (K)	$\dot{m}_{outer}$ (mg/s)	ρ_{outer} (kg/m^3)	u_{outer} (m/s)	Re_{outer} (10^4)	T_{inner} (K)	$\dot{m}_{inner}$ (mg/s)	ρ_{inner} (kg/m^3)	u_{inner} (m/s)	Re_{inner} (10^4)
2.0	6.9	246	21	1.49	195	450	27	6.6	1.1	109	925	630	0.96	1.5
5.2	11	217	24	1.49	184	750	29	10	1.9	110	925	620	0.97	1.5
12	17	222	23	1.49	194	1100	27	16	2.6	108	925	640	0.94	1.4
17	20	217	24	1.48	194	1300	27	19.3	3.1	108	925	638	0.95	1.4

$Pr = 1.05$, SAR

J	R	$T_{chamber}$ (K)	$\rho_{chamber}$ (kg/m^3)	$P_{chamber}$ (MPa)	T_{outer} (K)	$\dot{m}_{outer}$ (mg/s)	ρ_{outer} (kg/m^3)	u_{outer} (m/s)	Re_{outer} (10^4)	T_{inner} (K)	$\dot{m}_{inner}$ (mg/s)	ρ_{inner} (kg/m^3)	u_{inner} (m/s)	Re_{inner} (10^4)
9.4	9.9	214	59	3.58	203	1460	63	9.2	3.2	109	925	650	0.93	1.3
19	14	215	59	3.56	207	2060	62	13	4.5	111	925	635	0.95	1.4